A class of slipline field solutions for metal machining with slipping and sticking contact at the chip-tool interface

K.P. Maity *, N.S. Das

Department of Mechanical Engineering, Regional Engineering College, Rourkela, Orissa 769008, India

Abstract

In the present investigation slipline field solutions for orthogonal machining are presented when the plastically stressed region in the chip/tool contact length consists of both slipping ($\tau \leqslant k$) and sticking ($\tau = k$) zones. The interface friction in the slipping region is assumed to obey Coulomb's law and the fields are analysed using the linear approximation to the above non-linear boundary value problem as suggested by Dewhurst. The range of validity of the above slipline fields is examined from the consideration of overstressing of rigid vertices in the assumed rigid regions. Results are presented for variation of cutting forces, cutting ratio, chip curl radius and contact length with variation in rake angle and interface friction coefficient. Solutions incorporating elastic effects are obtained by the method suggested by Childs. Results from the theoretical analysis are compared with experimental values reported in literature.

Keywords: Metal-machining; Sticking-slipping contact; Slipline field solutions

1. Introduction

During metal machining the chip is subjected to high contact pressure/high traction conditions at the chip/tool interface due to sliding friction. As a result the friction stress attains the limiting value of yield stress k in shear over a portion of the plastically stressed contact region nearest to the cutting edge [1]. Experimental studies using a split tool carried out by Childs et al. [2], Barrow et al. [3], Kato et al. [4] and Buryta et al. [5] and photoelastic analysis of the machining process carried out by Chandrasekhar et al. [6], Bagchi et al. [7] and Usui and Takeyama [8] suggest that two zones exist on the face of the tool and these exhibit different frictional characteristics. In the zone adjacent to the tool tip, the high normal pressure results in the real area of contact between the rake face and the chip being equal to the apparent area

Nomenclature

$\theta, \eta, \eta_1, \delta, \psi$	slipline field angles
ϕ	friction angle as defined in Eq. (9)
p_E, p_A	hydrostatic pressures at E and A in the slipline fields
t_1, t_0	deformed chipthickness and undeformed chipthickness
l_s, l_e, l_t	sticking, elastic and natural contact length
γ	rake angle
k	yield stress in shear
σ_n, τ	normal stress and shear stress at the chiptool interface
μ	coefficient of friction in the zone of slipping contact
F_c, F_t	tangential cutting force and thrust force

of contact. Under these conditions the frictional stress is independent of the normal stress σ_n and is equal to the yield stress k in shear of the chip material. In this region of "sticking" friction, the classical Coulomb friction law fails. At the end of this zone the normal force on the rake face reduces to a value at which the real area of contact becomes less than the apparent. In this zone of "slipping/sliding" contact, the friction stress τ becomes less than k, σ_n and τ progressively decrease and finally becomes zero at the point at which the chip leaves the tool. It has been suggested that in this zone of slipping contact, Coulomb friction law holds (Worthington [9], Worthington and Redford [10], Wright and Thangaraj [11], Childs and Mahdi [2] and Hsu [12]).

Thus the friction law governing the chipflow in the above two zones are expressed by two independent equations which are written as,

$$\tau = \mu\sigma_n, \quad \mu\sigma_n \leqslant k, \tag{1a}$$

$$\tau = k, \quad \mu\sigma_n \geqslant k, \tag{1b}$$

where, μ is the Coulomb coefficient of friction in the slipping region.

Even though the length of plastic contact consists of both sticking ($\tau = k$) and slipping ($\tau \leqslant k$) regions, due consideration to this observation has not been accorded in the theoretical analysis of the machining process. In the slipline field solutions proposed by Lee and Shaffer [13] and Kudo [14] the interface friction was assumed to be governed either by Eqs. (1a) or (1b) so that the friction stress over the whole contact region was every where less than k (full slipping) or equal to k (full sticking). Similar assumptions about the nature of contact was also made in the slipline field analysis carried out by Dewhurst [15], Childs [16] and Sih and Ramalingam [17] though the chip formation in their study was assumed to take place under condition of constant friction stress ($\tau = mk$).

In the present analysis slipline field solutions for the machining process are presented assuming sticking and slipping contact in the plastically stressed region at the chip/tool interface. Coulomb friction is assumed in the zone of slipping contact and the chip is assumed to emerge from the deforming zone with an angular velocity (chip curl). With this friction law, however, the relation between the angular range of α- and β-lines bordering the slipping region becomes non-linear. Using linear approximation to this non-linear relation, the solutions are constructed

by the matrix methods developed by Dewhurst [18] and Dewhurst and Collins [19]. It is shown that sticking begins when the coefficient of friction exceeds a certain minimum value. Length of sticking and slipping regions and the interface stress distribution are computed as a function of the coefficient of friction for different tool rake angles. Results for cutting and thrust forces, chip curvature and cutting ratio are also presented. The computed values are also compared with some experimental results available in literature.

Though the analysis presented here assumes Coulomb friction in the zone of slipping contact, the method proposed is quite general in nature and is easily extended to deal with any other linear/non-linear friction boundary condition at the chip/tool interface.

2. Slipline field solutions

Two slipline fields which cover the complete range of friction conditions encountered in metal machining are shown in Figs. 1 and 2 along with their associated hodographs.

Solution I (Fig. 1) is the modified Dewhurst field [15] when Coulomb friction obtains on the interface CE. The solution applies when the friction stress τ on the chip/tool boundary no where equals the yield stress k in shear ($\tau \leqslant k$). This condition is satisfied when for any given value of the coefficient of friction μ, the angular range η of the α-line ED is less than the limiting value η_L given by the equation

$$\eta_L = (1/\mu - p_E - 2\phi_E)/4, \tag{2}$$

where, p_E is the hydrostatic pressure at E and ϕ_E is the angle at which slipline ED meets the tool face.

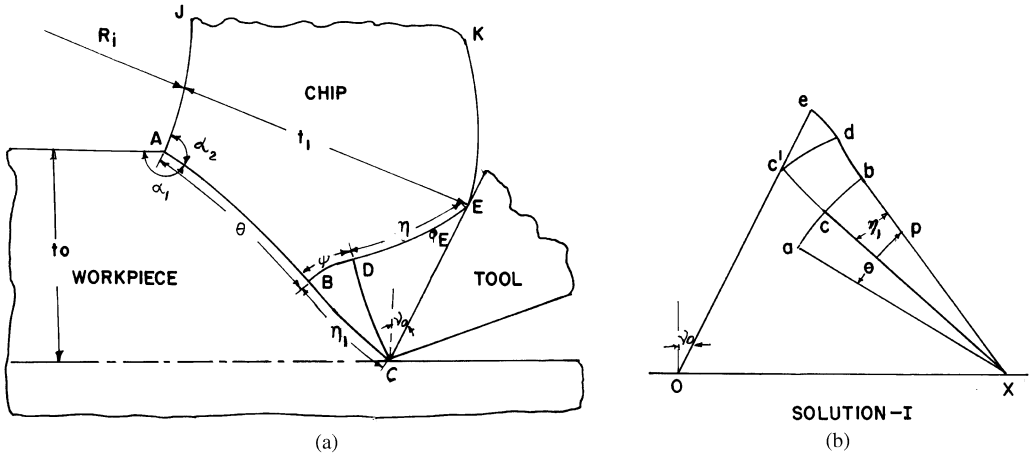

Fig. 1. (a) Slipline field of Solution I; (b) hodograph for slipline field in Fig. 1(a).

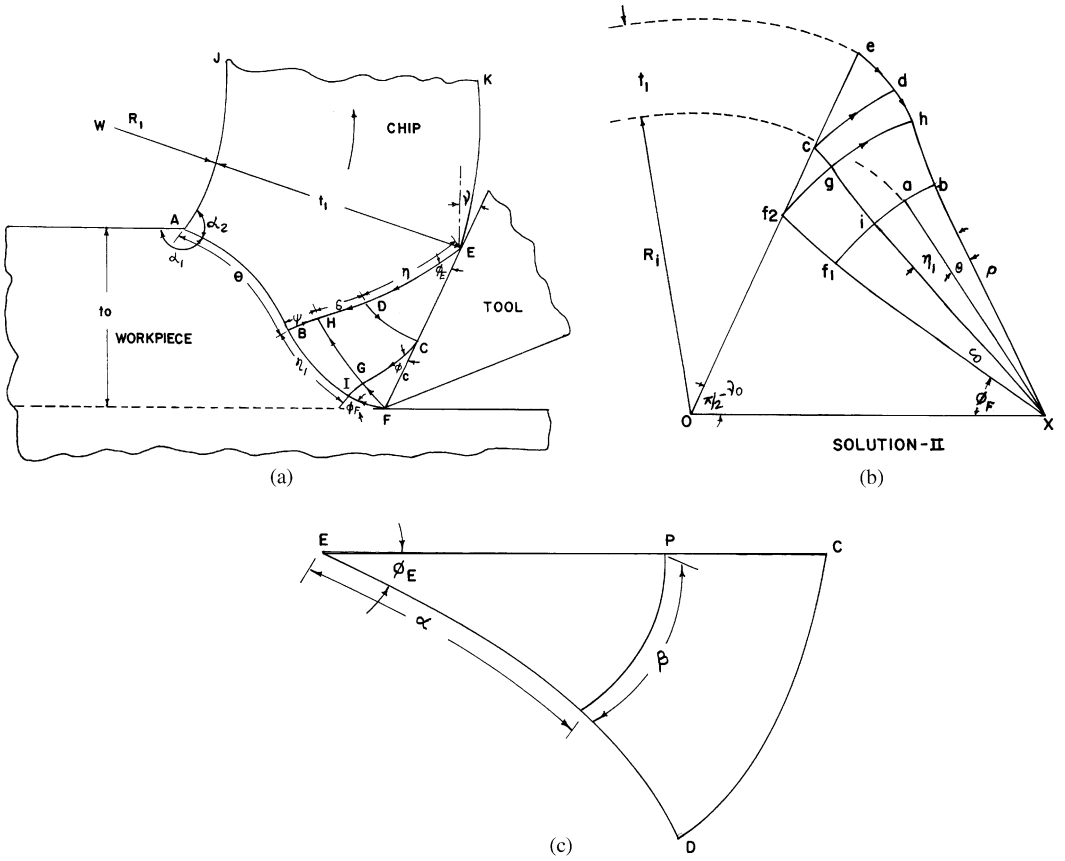

Fig. 2. (a) Slipline field of Solution II; (b) hodograph for slipline field in Fig. 2(a); (c) angular coordinates of slipline fields.

It is seen that in order for the slipline field to satisfy the mixed stress and velocity boundary conditions, slipline ED(σ_1) must satisfy the matrix equation (refer to the appendix),

$$(I - \mathrm{CL}_{\eta_1\phi_c} Q_{\psi\eta_1} Q_{\eta_1\psi} \mathrm{CL}_{\eta\phi_E})\sigma_1 = (\rho/\omega)\mathrm{CL}_{\eta_1\phi_c} P_{\eta_1\psi}\bar{c}, \tag{3}$$

where CL is the Coulomb operator [18], P and Q are standard matrix operators [19], ρ is the velocity discontinuity across the primary shear line CBA and ω is the angular velocity with which the chip rotates on leaving the deformation zone (Fig. 1(b)).

When the angular range of the α-line ED attains the limiting value η_L given by Eq. (1), both sticking and slipping regions may be present in the chip/tool contact length. The slipline field that satisfies this requirement is shown in Fig. 2 (solution II). EDC and CGF in the above figure define the slipping and sticking zones, respectively, with $\tau \leqslant k$ on EC and $\tau = k$ on CF, while FGI is the singular field constructed about point F. Referring to the corresponding hodograph shown in Fig. 2(b), it is demonstrated that all velocity boundary conditions are also satisfied.

The matrix equation defining the base slipline BH (σ_3) in this case is written as

$$(I - (UZ + VX))\sigma_3 = (\rho/\omega)(UY + VW)\bar{c}, \tag{4}$$

where I is the unit matrix, $\bar{c}$ is the column vector representing a unit circle and U, V, W, X, Y, Z are resultant matrix operators as derived in the appendix.

It may be noticed that both these fields have four degrees of freedom given by the field angles θ, ψ, η/δ and the hydrostatic pressure p_E. Since there are only three stress boundary conditions to be satisfied for a force free chip, both these fields are non-unique in nature.

It may be seen that the angular coordinates of any point P on the slipping region EC (Fig. 2(c)) are governed by the equation

$$\mu(p_E/k + 2(\alpha + \beta) + \sin 2(\phi_E + \alpha - \beta)) - \cos 2(\phi_E + \alpha - \beta)) = 0. \tag{5}$$

Following Dewhurst [18] the above non-linear relation was approximated by a linear relation given by

$$\beta = m_0\alpha. \tag{6}$$

For low values of μ, an approximate expression for m_0 was presented by Dewhurst [18] based on small angle approximation. However, as reported by Murakami [20] this gives rise to large error when μ exceeds 0.3.

In the present study m_0 was calculated using the method of linear regression analysis. For points with known angular coordinates α on ED, the corresponding β values were calculated by solution to Eq. (5) by Newton-Raphson method. These data were then used to calculate m_0 from the equation

$$m_0 = \sum_{i=1}^{j} \alpha_i^2 \Big/ \sum_{i=1}^{j} \beta_i\alpha_i, \tag{7}$$

where α_i, β_i are the coordinates of any arbitrary point on ED. Calculation was carried out by taking ten points on ED ($j = 10$).

If the interface friction is assumed to be governed either by the linear friction law $\tau = mk$ or by the adhesion friction law given by the equation,

$$\tau = k(1 - e^{-(\mu\sigma_n/k)}), \tag{8}$$

the friction stress no where equals the yield stress k in shear ($\tau \leqslant k$) in the chip/tool contact region. For these cases, therefore, slipline field shown in (Fig. 1(a)) satisfies the necessary boundary requirements on stress and velocity and the base slipline can be computed by solution to Eq. (3). The linear coefficient m_0 (Eq. (6)) for constructing the Coulomb operator CL, however, is to be suitably calculated consistent with the assumed friction condition. For the linear friction law, $m_0 = 1$. For the adhesion friction law, the value of m_0 should be determined with the help of Eqs. (8) and (7).

3. Computation of slipline fields

The slipline fields shown in Figs. 1 and 2 are of indirect type and these were analysed by solutions to the matrix Eqs. (3) and (4). A FORTRAN program developed for the purpose

required input of friction coefficient μ, hydrostatic pressure p_E at E and an initial guess for the three field angles θ, ψ and η/δ. The program first evaluated ϕ_E by solution to the equation

$$\mu(p_E/k + \sin 2\phi_E) - \cos 2\phi_E = 0 \tag{9}$$

and then determined the linear coefficient m_0 (Eq. (7)). These data were used to generate Coulomb and basic matrix operators and determine the column vector for the base slipline. Other slipline and hodograph curves were now calculated and the forces F_1, F_2 and moment M on the chip boundary ABED evaluated. The field angles were calculated from the requirement of force free condition of the chip. An algorithm developed by Powell [21] for solution to non-linear algebraic equations was employed for the purpose and free chip condition was assumed to be satisfied when the values of the field angles $\theta, \psi, \eta/\delta$ satisfied the inequality

$$(F_1/kt_0)^2 + (F_2/kt_0)^2 + (M/kt_0^2)^2 \leqslant 10^{-10}. \tag{10}$$

In all calculations, the scale factor ρ/ω was set equal to 1. The programme also incorporated the following checks to test the accuracy of calculations:

(i) Flatness check: Point C on slipline curve DC (Fig. 1 (a)) and points C, F on slipline curves DC, GF (Fig. 2(a)), respectively, must lie on the tool face. Similarly point e on hodograph curve de must lie on line oc′ (Fig. 1(b)) or line oc (Fig. 2(b)).

(ii) Mass flux check: The mass entering into the deformation region should be equal to mass leaving the same. This is written as

$$t_1 \cdot (\mathrm{oe} + \mathrm{oa})/2 = \mathrm{to} \cdot \mathrm{ox}. \tag{11}$$

(iii) Traction check: The horizontal and vertical forces calculated from the primary shear line CBA (Fig. 1(a)) or FBA (Fig. 2(a)) should be equal to those calculated from the sliplines bordering the plastically stressed region (EB and CB for solution I and ED, CD and CG, FG for solution II).

In all calculations the above three requirements were found to be satisfied to 5 significant figures.

In the present study it was assumed that $\tau = k$ on CF ($\phi_E + \eta - \eta_1 = 0$, Fig. 2(a)). Due to the linear approximation, $\beta = m_0\alpha$, however it was not found to be so and τ differed marginally from k. For $\mu = 0.6$, τ was equal to 0.995k and for $\mu = 0.8$, τ was equal to 0.998k. Attempt was also made to analyse the fields by the method proposed by Murakami [20] by fitting a cubic polynomial between the angular range of α- and β-lines given by the equation

$$\beta = m_1\alpha + m_2\alpha^2 + m^3\alpha^3, \tag{12}$$

where m_1, m_2 and m_3 were calculated by Langrange interpolation. But with this procedure the solution did not converge for a value of μ as low as 0.4 even with matrices of size 20×20. This was because coefficients in Eq. (12) generally diverge and m_2, m_3 become very large as μ increases. This method of analysis was therefore not pursued further. It is also likely that no significant improvement will result when τ has a value exactly equal to k on CF (Fig. 2(a)).

4. Range of validity

Not all solutions given by the present slipline fields are necessarily valid. For this to be so the plastic stress field must be extended to the chip and the workpiece to demonstrate that the yield criterion is not violated in the rigid regions. This requires that the hydrostatic pressure p_A at A should be such that the rigid vertices at A are not overstressed. Following Hill [22] the range of permissible values of p_A for which valid solutions are obtained is written as

$$p_A/k \leqslant 1 - 2\cos(\alpha_1 - \pi/4), \quad \alpha_1 \leqslant 3\pi/4,$$
$$p_A/k \leqslant 1 + 2(\alpha_1 - 3\pi/4), \quad \alpha_1 \geqslant 3\pi/4, \tag{13}$$

and

$$1 + 2(\alpha_2 - \pi/4) \geqslant p_A/k \geqslant -1 + 2\cos(\alpha_2 - /4), \quad \alpha_2 \geqslant \pi/4.$$

In some solutions, point f_2 in the hodograph diagram (Fig. 2(b)) was found to be below the line ox. This occurred for large values of μ ($\geqslant 0.6$) and for tool rake angles γ less than 5°. The cutting ratio and the cutting forces for these solutions were also found to be large. It is likely that formation of built up edge takes place under these conditions.

5. Results and discussion

For any given value of μ and hydrostatic pressure p_E, as the angular range η of slipline ED increases, field angles θ and ψ also increase (Fig. 1(a)). At low values of μ (< 0.55) the rigid vertices at A are overstressed before η attains the limiting value η_L (Eq. (2)). Under these conditions the machining behavior is governed by solution I only. The range of validity for $\mu = 0.25$ is given in Fig. 3(a), defined in terms of the possible range of ψ, the angle of the centre fan. Referring to the above figure, it may be seen that the upper limit on ψ for this case is given by the curve UL, where the field angles produce overstressing of vertex angle α_2 (Fig. 1(a)). For γ greater than 12°, the lower limit on ψ is given by the curve LL which refers to the overstressing of vertex angle α_1. It is also seen that for γ less than 12°, Lee and Shaffer's solution [13] defines the lower limit. Thus it appears that for the given value of μ chip will always leave the deformation zone with a curvature when γ exceeds 12°. For still lower values of μ, curve LL shifts to the left and eventually meets the abscissa at γ equal to 0° for $\mu = 0.0$. For higher values of μ the above curve shifts to the right. It was also observed that for $\mu > 0.4$, vertex angle α_1 is never overstressed for the range of rake angles examined.

Solutions with slipping and sticking zones in the chip/tool contact length are predicted only when $\mu \geqslant 0.55$. The permissible range of values of ψ for such a case for $\mu = 0.6$ is shown in Fig. 3(b). Referring to the above figure, it may be seen that the lower limit for all rake angles in this case is provided by Lee and Shaffer's solution [13] for which $\psi = 0$. The upper limit on ψ for slipping contact only is indicated by the curve SL in the above figure for which η has a value equal to η_L in solution I (Fig. 1(a)). This curve is nearly flat as for any given value of μ the field angles are independent of the tool rake angle. This observation was also reported earlier by Dewhurst [15]. When the contact length involves both slipping and sticking zones the maximum permissible value of ψ is restricted by overstressing of vertex angle α_2 in

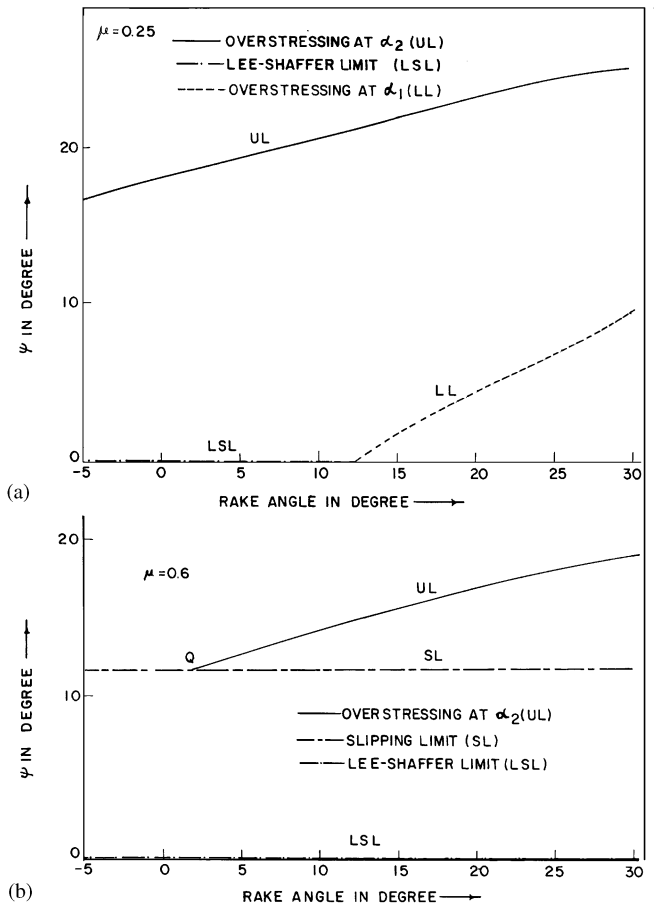

Fig. 3. (a) Range of validity of slipline field in Fig. 1(a); (b) range of validity of slipline field Fig. 2(a).

solution II (Fig. 2(a)). This is indicated by the curve UL in Fig. 3(b). It may also be seen that the curves UL and SL meet at point Q corresponding to γ equal to 2°. Thus for machining with tools having rake angle less than the above value, the interface will be governed by slipping friction only.

The variation of machining parameters with rake angle as obtained from the present analysis are shown in Figs. 4–8 for μ values equal to 0.0, 0.4, 0.6 and 0.8. For each value of the rake angle, the range of possible solutions lie within the limits as discussed with reference to Fig. 3. Referring to the above figures, it may be seen that the rake angle and the interface friction are the two most important variables in metal machining that influence the cutting forces, cutting ratio and chip curvature. The cutting and thrust forces and cutting ratio are found to decrease with increase in γ and with decrease in the value of μ which is in agreement with experimental observations. It may also be seen that chip curvature (t_0/Rm) decreases as μ value increases indicating that the chip will have a tendency to stream rather than curl as rake friction increases (Fig. 6). The computed values of the cutting ratio are compared with the experimental results

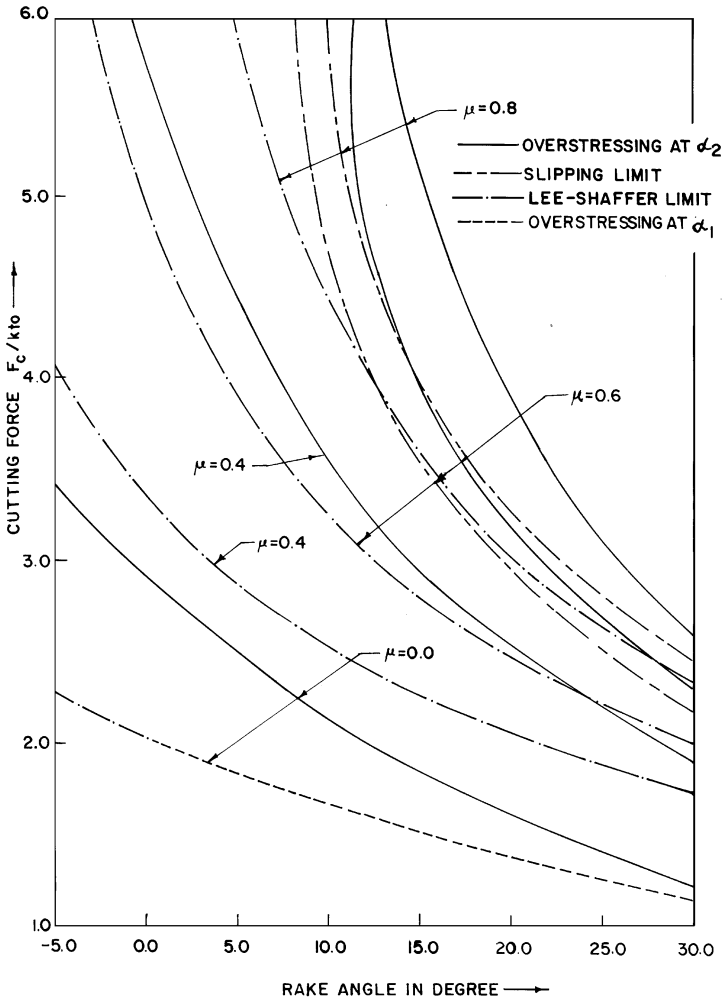

Fig. 4. Variation of non-dimensionaized cutting force with γ and μ.

of Eggleston et al. [23] in Fig. 7. Referring to this figure, it may be seen that there is excellent agreement between theory and experiment for all rake angles with the experimental points mostly lying within the solution range for $\mu = 0.4$ and 0.8.

The variation of non-dimensional contact length l_t/t_0, the non-dimensional sticking length l_s/t_o and sticking ratio l_s/l_t with rake angle is shown in Fig. 8 where, it is also compared with the experimental results reported in references [4,6,23–25]. For $\gamma = 5^\circ$, 10° and 15°, most of the experimental points are found to lie within the solution range for $\mu = 0.4$ and 0.8. At higher rake angles, however, the agreement between theory and experiment is not found to be so good. Better agreement may be obtained when a higher value of μ is assumed for these cases. It may also be seen with reference to Fig. 8 that though l_t/t_0 and l_s/t_0 vary, the sticking ratio l_s/l_t is virtually unaffected by variation in rake angle.

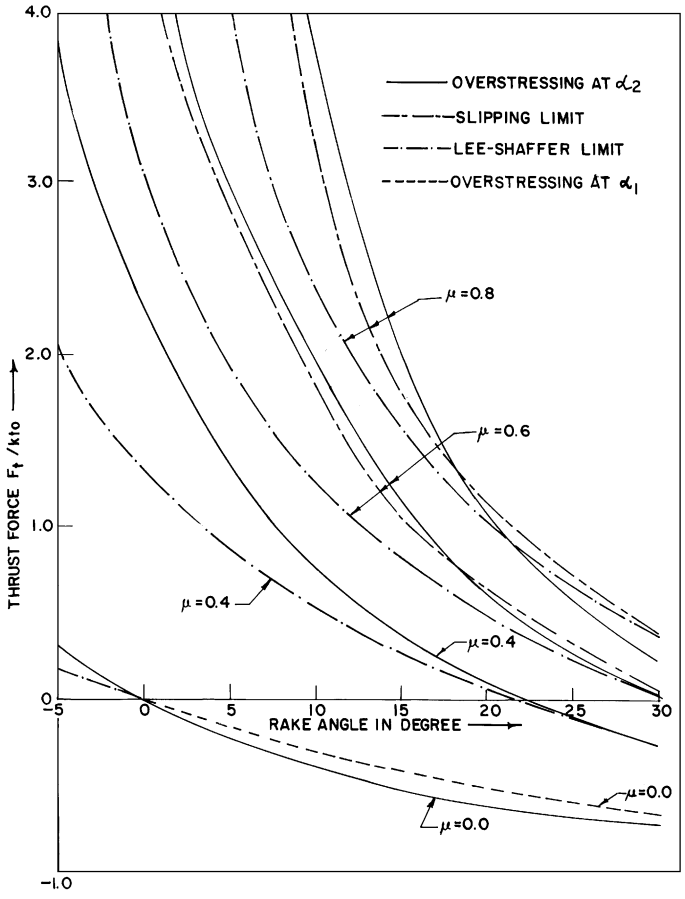

Fig. 5. Variation of non-dimensionalized thrust force with γ and μ.

It is observed that the predicted variations in the machining parameters depend critically upon the choice of the tool rake angle (Figs. 4–8). The range of possible solutions decrease as the rake angle increases.

6. Solutions with elastic contact

Contact stress distribution on the tool rake face obtained from photoelastic analysis [6–8] or using a split tool [2–5] suggest that in metal machining there usually exists an extensive region of elastic contact beyond the zone of plastic contact the forces acting across which contribute significantly to the cutting and thrust forces. To incorporate this elastic effect into the present analysis an elastic contact length beyond the length of plastic contact was assumed as suggested by Childs [16]. In the plastic zone the normal and shear stresses were assumed to be governed by the proposed slipline fields. In the length of elastic contact the normal pressure was assumed

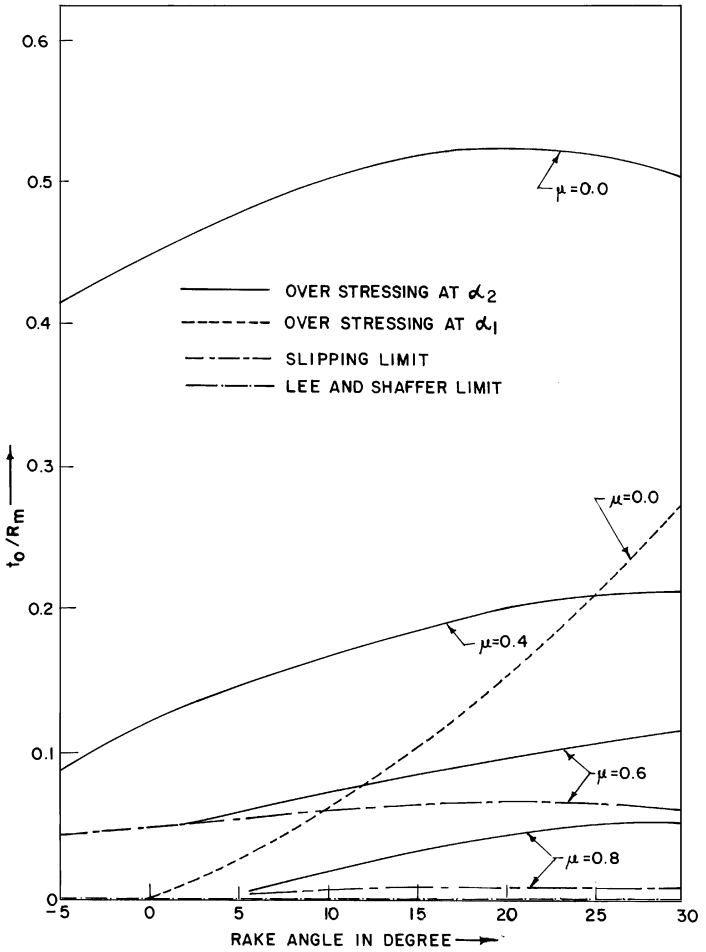

Fig. 6. Variation of curvature of the machined chip with γ and μ.

to be distributed either exponentially or parabollically thus giving rise to a resultant force and a moment. The field angles were determined in the same way as for free chip formation from equilibrium consideration such that the force and moment due to the slipline curves bordering the chip were equal and opposite to those generated in the elastic contact length. The solution procedure is discussed in detail in Ref. [26]. The range of validity of these solutions were again determined from the consideration that the vertex angles α_1 and α_2 are not overstressed.

Incorporation of an elastic contact length introduces an additional variable to the slipline fields over and above the existing four $(\theta, \psi, \eta/\delta, p_E)$ as discussed in Section 2. Since there are only three stress boundary conditions to be satisfied $(F_1 = F_2 = M = 0)$ the fields in this case are also non-unique.

Incorporation of elastic effects were found to extend the solution range from the proposed fields and this is in agreement with the observations made earlier by Childs [16]. Thus, the experimental points for tool/chip contact length for higher rake angles which were outside the

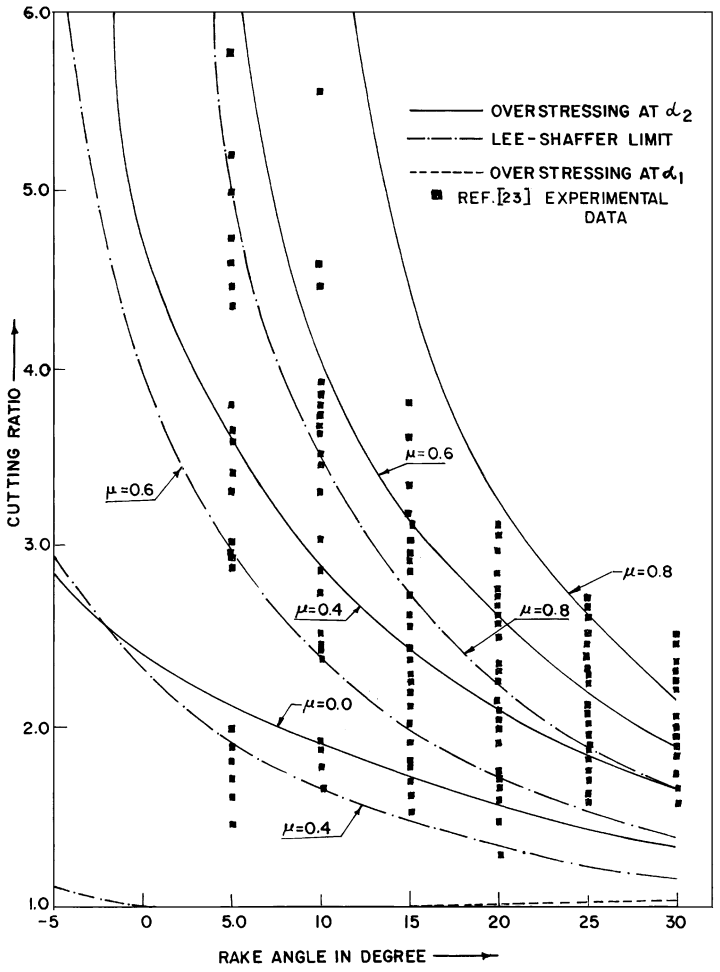

Fig. 7. Variation of the cutting ratio with γ and μ.

solution range in Fig. 8 considering plastic contact only were now found to be within the solution range when elastic and plastic contact was considered.

A typical plot of stress distribution with elastic and plastic contact at chip/tool interface is shown in Fig. 9. The distribution is for the limiting situation where for the given rake angle γ and friction coefficient μ the field angles produce overstressing of the vertex angle α_2. The normal stress σ_n within the elastic zone in the above figure is assumed to be governed by the exponential relation

$$\sigma_n = \sigma_0(1 - e^{nl/l_e})/(1 - e^n), \tag{14}$$

where σ_0 is the normal pressure on the tool at the elastic/plastic transition point, l_e is the length of elastic contact, l is the distance of the point under consideration from the point of chip separation ($l < l_e$) and n is constant. For the above plot l_e was assumed equal to the length of plastic contact and the value of n was set equal to 1. With these values the computed

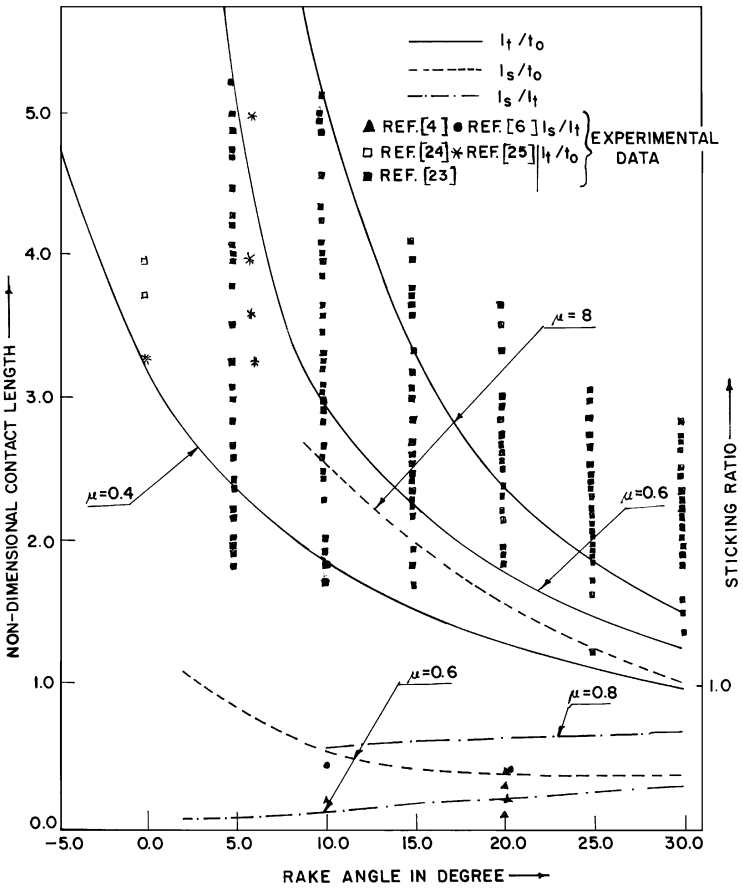

Fig. 8. Variation of l_t/t_0, l_s/t_0 and l_s/l_t with γ and μ.

elastic forces were within 30–40% of the total cutting force for $\mu = 0.8$ and the length of plastic contact was 50% of the natural contact length which is consistent with experimental observations [6].

Referring to the above figure it may be seen that for $\mu = 0.4$ the normal pressure increases monotonically in the length of plastic contact. The same trend is also observed for $\mu = 0.6$ and 0.8, though the rise in pressure is not as steep in the zone of slipping contact as it is in the sticking contact area. It may also be seen that the extent of sticking contact is very much influenced by the value of μ. At $\mu = 0.6$, the length of sticking contact forms only 25% of the length of total plastic contact, which increases to 70% for $\mu = 0.8$. Even within the slipping contact zone τ does not differ much from k, the least value being $0.94k$ for $\mu = 0.8$. This may be the reason why the distribution of τ in the plastic contact area from experimental measurements appears to be nearly flat.

The contact stress distribution shown in Fig. 9 refers to the upper limiting values for the cutting conditions indicated ($\gamma = 30^0$, $\mu = 0.4$, 0.6 and 0.8). The lower limit to the stress distribution are again provided by Lee and Shaffer's solution [13]. For this case both

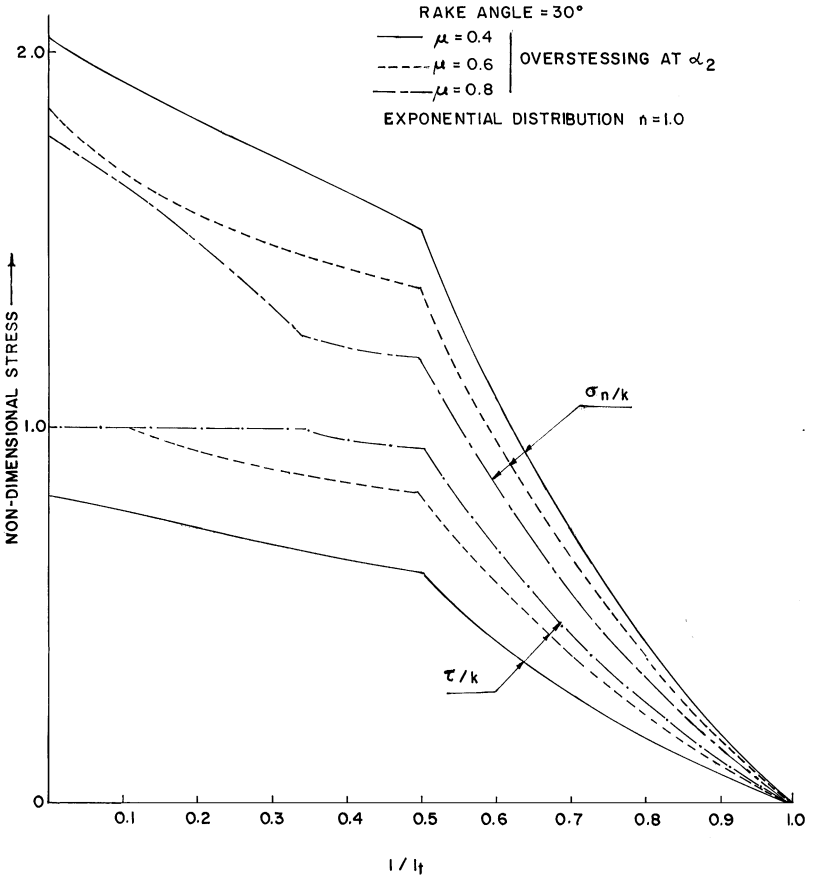

Fig. 9. Variation of σ_n and τ at the chip-tool interface.

normal and shear stresses along the rake face are constant and the elastic contact length is zero [26]. Depending on the condition of cutting, the contact stresses are expected to lie within these limits.

7. Conclusions

In the present analysis slipline field solutions for the orthogonal machining process are presented assuming sticking and slipping contact in the plastically stressed region at the chip/tool interface. Interface friction within the zone of slipping contact is assumed to obey Coulomb's law and the solutions are constructed by linear approximation to this non-linear boundary value problem as suggested by Dewhurst. Limits of validity of these solutions have been examined by applying Hill's overstressing criterion.

It is seen that for a given value of friction coefficient $\mu \leqslant 0.55$ the interface friction results in slipping contact only. When μ exceeds the above value, sticking and slipping zones are predicted

in the length of plastic contact. Solutions with slipping contact can be obtained by analysis of the modified Dewhurst field shown in Fig. 1. The slipline field shown in Fig. 2 applies when the plastically stressed region in the interface consists of both slipping and sticking zones. Solutions incorporating elastic effects have also been constructed by introducing a length of elastic contact beyond the plastically stressed region as suggested by Childs.

Computed values of machining parameters such as cutting force, thrust force, cutting ratio, chip curvature and contact length are presented for rake angle values between -5° and 30° and for μ values between 0 and 0.8. For any given value of rake angle and friction coefficient μ, the solutions are found to lie within the limits imposed by the overstressing of assumed rigid regions in the chip and the workpiece. Tool rake angle and interface friction are seen to have most significant influence on machining parameters. The predicted variations in the machining parameters depend critically upon the choice of the tool rake angle. The range of possible solutions decrease as rake angle increases.

Computed values of cutting ratio and contact length are found to show excellent agreement with experimental results reported in literature.

Acknowledgements

A fruitful discussion with Professor T.H.C. Childs by Prof K.P. Maity during his stay in U. K. regarding implementation of Coulomb friction at the chip-tool interface in metal machining in slipline field analysis is duly acknowledged. Authors are also grateful to the system-manager, computer centre, REC Rourkela for providing facilities to run the programmes.

Appendix

Matrix Eq. (3) for solution I is derived as follows:

Referring to Fig. 1(a), let the column vector for the base slipline ED be denoted by σ_1. Hence,

$$\mathrm{CD} = \mathrm{CL}_{\eta\phi_\mathrm{E}}\sigma_1, \tag{A.1}$$

where CL is the Coulomb operator as defined in [18]. Thus,

$$\mathrm{BD} = Q_{\eta_1\psi}\mathrm{CL}_{\eta\phi_\mathrm{E}}\sigma_1. \tag{A.2}$$

Referring now to the hodograph diagram shown in Fig. 1(b), because of the rigid body rotation of the chip, the geometrical similarity of sliplines ABDE and the corresponding hodograph curves may be expressed as

$$\mathrm{bd} = \omega Q_{\eta_1\psi}\mathrm{CL}_{\eta\phi_\mathrm{E}}\sigma_1 \tag{A.3}$$

and

$$\mathrm{ed} = \omega\sigma_1, \tag{A.4}$$

where ω is the angular velocity of chip curl.

The material on entering the deformation zone suffers a velocity discontinuity of magnitude ρ as shown in Fig. 1(b). Thus circular arc bc is written as

$$\mathrm{bc} = \rho\bar{c}. \tag{A.5}$$

The curve c′d in the hodograph is calculated from bc and bd (superposition principle) using the relation

$$\mathrm{c'd} = P_{\eta_1\psi}\rho\bar{c} + Q_{\psi\eta_1}\omega Q_{\eta_1\psi}\mathrm{CL}_{\eta\phi_\mathrm{E}}\sigma_1. \tag{A.6}$$

Also

$$\mathrm{ed} = \mathrm{CL}_{\eta_1\phi_\mathrm{E}}\mathrm{c'd} \tag{A.7}$$

Using Eqs. (A.4), (A.6) and (A.7) the matrix equation determining σ_1 is finally written as

$$(I - \mathrm{CL}_{\eta_1\phi_\mathrm{c}}Q_{\psi\eta_1}Q_{\eta_1\psi}\mathrm{CL}_{\eta\phi_\mathrm{E}})\sigma_1 = (\rho/\omega)\mathrm{CL}_{\eta_1\phi_\mathrm{c}}P_{\eta_1\psi}\bar{c}, \tag{3}$$

where, I is the unit matrix, $\bar{c}$ is a column vector representing unit circle and P, Q are standard matrix operators as defined in [19].

The matrix Eq. (4) for solution II may be derived in the following manner:

Let the sliplines ED, DH and BH in Fig. 2(a) be denoted by the column vectors σ_1, σ_2 and σ_3, respectively. Hence,

$$\mathrm{CD} = \mathrm{CL}_{\eta\phi_\mathrm{E}}\sigma_1 \quad \text{and} \quad \mathrm{DC} = R_{\eta_1}\mathrm{CL}_{\eta\phi_\mathrm{E}}\sigma_1. \tag{A.8}$$

Curves GH and CG can be defined from curves DC and DH as

$$\begin{aligned} \mathrm{GH} &= P_{\eta_1\delta}\mathrm{DC} + Q_{\delta\eta_1}\sigma_2, \\ \mathrm{CG} &= P^*_{\eta_1}\sigma_2 + Q^*_{\eta_1}\mathrm{DC}. \end{aligned} \tag{A.9}$$

Since friction stress τ is constant on CF, FG is calculated from CG using the rough boundary operator. This relation is written as

$$\mathrm{FG} = G_{\delta\phi_\mathrm{c}}\mathrm{CG}. \tag{A.10}$$

FGI is a singular field. Hence,

$$\mathrm{GI} = Q^*_\delta\mathrm{FG}. \tag{A.11}$$

BH (σ_3) is finally derived from slipline curves GH and GI using the relation,

$$\sigma_3 = P_{\psi\eta_1}\mathrm{GI} + Q_{\eta_1\psi}\mathrm{GH}. \tag{A.12}$$

Substituting Eqs. (A.8), (A.9), (A.10) and (A.11) in equation (A.12), σ_3 is finally expressed in terms of σ_1 and σ_2. This is written as

$$\sigma_3 = U\sigma_2 + V\sigma_1, \tag{A.13}$$

where U and V are resultant matrix operators defined as

$$U = P_{\psi\eta_1}Q^*_\delta G_{\delta\phi_\mathrm{c}}P^*_{\eta_1} + Q_{\eta_1\psi}Q_{\delta\eta_1}$$

and

$$V = P_{\psi\eta_1}Q^*_\delta G_{\delta\phi_\mathrm{c}}Q^*_\delta R_{\eta_1}\mathrm{CL}_{\eta\phi_\mathrm{E}} + Q_{\eta_1\psi}P_{\eta_1\delta}R_{\eta_1}\mathrm{CL}_{\eta\phi_\mathrm{E}}. \tag{A.14}$$

Referring now to Fig. 2(b), rigid body rotation of the chip requires that the hodograph curves bh, dh and ed are geometrically similar to their slipline images. Thus,

$$\mathrm{ed} = \omega\sigma_1, \quad \mathrm{dh} = \omega\sigma_2 \quad \text{and} \quad \mathrm{bh} = \omega\sigma_3. \tag{A.15}$$

Further, bf_1 is a circular arc of radius ρ, the velocity discontinuity across the primary shear line FIBA. Therefore, bf_1 is written as

$$\mathrm{bf}_1 = \rho\bar{c}. \tag{A.16}$$

Curve $\mathrm{f}_2\mathrm{h}$ can be defined from curves bh and bf_1 as

$$\mathrm{f}_2\mathrm{h} = P_{\xi\psi}\rho\bar{c} + Q_{\psi\xi}\omega\sigma_3, \tag{A.17}$$

where

$$\xi = \eta + \delta.$$

Also gh and gc are calculated from $\mathrm{f}_2\mathrm{h}$. These relations are written as

$$\mathrm{gh} = S_\delta \mathrm{f}_2\mathrm{h} \quad \text{and} \quad \mathrm{gc} = R_\delta G_{\delta\phi_\mathrm{c}} \mathrm{f}_2\mathrm{h} \tag{A.18}$$

Curves cd and dh can be defined from curves gc and gh,

$$\begin{aligned} \mathrm{dh} &= \omega\sigma_2 = P_{\delta\eta_1}\mathrm{gc} + Q_{\eta_1\delta}\mathrm{gh} \\ \mathrm{cd} &= Q^*_\delta \mathrm{gc} + P^*_\delta \mathrm{gh} \end{aligned} \tag{A.19}$$

Further, ed is calculated from cd using the Coulomb operator. Thus,

$$\mathrm{ed} = \omega\sigma_1 = \mathrm{CL}_{\eta_1\phi_\mathrm{c}}\mathrm{cd} \tag{A.20}$$

Substituting Eqs. (A.16)–(A.18) in Eqs. (A.19) and (A.20), σ_1 and σ_2 are finally expressed in terms of σ_3. These relations are written as

$$\sigma_1 = X\sigma_3 + \rho/\omega W\bar{c} \quad \text{and} \quad \sigma_2 = Z\sigma_3 + \rho/\omega Y\bar{c}, \tag{A.21}$$

where, W, X, Y and Z are operators given by the relations,

$$\begin{aligned} W &= \mathrm{CL}_{\eta_1\phi_\mathrm{c}} Q^*_\delta R_\delta G_{\delta\phi_\mathrm{E}} P_{\xi\psi} + \mathrm{CL}_{\eta_1\phi_\mathrm{c}} P^*_\delta S_\delta P_{\xi\psi}, \\ X &= \mathrm{CL}_{\eta_1\phi_\mathrm{c}} Q^*_\delta R_\delta G_{\delta\phi_\mathrm{c}} Q_{\psi\xi} + \mathrm{CL}_{\eta_1\phi_\mathrm{c}} P^*_\delta S_\delta Q_{\psi\xi}, \\ Y &= P_{\delta\eta_1} R_\delta G_{\delta\phi_\mathrm{c}} P_{\xi\psi} + Q_{\eta_1\delta} S_\delta Q_{\psi\eta}, \\ Z &= P_{\delta\eta_1} R_\delta G_{\delta\phi_\mathrm{c}} Q_{\psi\eta} + Q_{\eta_1\delta} S_\delta Q_{\psi\xi}. \end{aligned} \tag{A.22}$$

Substituting Eq. (A.21) in Eq. (A.13) the matrix equation for σ_3 is finally written as

$$(I - (UZ + VX))\sigma_3 = \rho/\omega(UY + VW)\bar{c}. \tag{4}$$

References

[1] Zorev NN. Interrelationship between shear processes occurring along tool face and on shear plane in metal cutting. Proc. Conf. Int. Res. Prod. Engg, ASME, New York, 1963. p. 42.

[2] Childs THC, Mahdi MI. On the stress distribution between the chip and tool during metal cutting. Annals CIRP 1989;38:55–8.
[3] Barrow G, Graham W, Kurimoto T, Leong YF. Determination of rake face stress distribution in orthogonal machining. International Journal of Machine Tool Design and Research 1982;22(1):75–85.
[4] Kato S, Yamaguchi K, Yanda M. Stress distribution at the interface between tool and chip in machining. Transaction of ASME Journal of Engineering Industry 1972;94(5):683–9.
[5] Buryta D, Sowerby R, Yellowley I. Stress distribution on the rake face during orthogonal machining. International Journal of Machine Tools Manufacture 1994;34(5):721–39.
[6] Chandrasekaran H, Kapoor DV. Photoelastic analysis of tool-chip interface stresses. Journal of Engineering Industry 1965;87(11):495–502.
[7] Bagchi A, Wright PK. Stress analysis in machining with the use of sapphire tools. Proceedings of Royal Society, London 1987;A409:99–113.
[8] Usui E, Takeyama H. A photoelastic analysis of machining stress. Transaction of ASME Journal of Engineering Industry 1960;82:303–8.
[9] Worthington B. The effect of rake face configuration on the curvature of the chip in metal cutting. International Journal of Machine Tool Design and Research 1975;15:221–9.
[10] Worthington B, Redford AH. Chip curl and the action of the groove type chip former. International Journal of Machine Tool Design and Research 1973;15:221–2.
[11] Wright PK, Thangaraj A. Correlation of tool wear mechanism with new slipline fields for cutting. Wear 1982;75:105–22.
[12] Hsu TC. A study of the normal and shear stresses on a cutting tool. ASME Journal of Engineering for Industry 1966;16:51–64.
[13] Lee EH, Shaffer BW. The theory of plasticity applied to a problem of machining. Journal of Applied Mechanics 1951;18:405.
[14] Kudo H. Some new slip-line solutions for two dimensional steady-state machining. International Journal of Mechanical Sciences 1965;7:43–55.
[15] Dewhurst P. On the non-uniqueness of the machining process. Proceedings of Royal Society, London 1978;A360:587–610.
[16] Childs THC. Elastic effects in metal cutting chip formation. International Journal of Mechanical Sciences 1980;22:457–66.
[17] Shi T, Ramalingam S. Slip-line solution for orthogonal cutting with a chip breaker and flank wear. International Journal of Mechanical Sciences 1991;33(9):689–774.
[18] Dewhurst P. The coulomb friction boundary value problem in plane-strain slipline field theory. Advanced Technology of Plasticity 1984;II:1085–90.
[19] Dewhurst P, Collins IF. A matrix technique for constructing slip-line field solutions to a class of plane strain plasticity problems. International Journal for Numerical Methods in Engineering 1973;7:357–78.
[20] Murakami T. A series method for non-linear boundary value problems in a slipline field theory. International Journal of Mechanical Sciences 1988;30(6):383–454.
[21] Kuester JL, Mize JH. Optimization techniques with FORTRAN. New York: Mc-Graw Hill, 1973.
[22] Hill R. On the limits set by plastic yielding to the intensity of singularities of stress. Journal of Mechanics and Physics of Solids 1954;2:278–85.
[23] Eggleston DM, Herzog R, Thomsen EG. Observations on the angle relationships in metal cutting. Transactions of ASME 1959;B-81:263–73.
[24] Pearce DF, Richardson DB. Machining stability using controlled contact tools. International Journal of Production Research 1975;13(1):75–82.
[25] Chiffre LD. Cutting tools with restricted contact. International Journal of Machine Tool Design and Research 1982;22(4):321–32.
[26] Maity KP, Das NS. A class of slipline field solutions for metal machining with elastic contact. Journal of Materials Processing Technology 1999;96(1–3):9–18.